An experimental investigation on fluidic behaviors in a two-dimensional nanoenvironment

Hui Li,[1,a)] Xiang Xu,[1,2] and Yu Qiao[2]
[1]*Center of Structural Monitoring & Control, School of Civil Engineering, Harbin Institute of Technology, Harbin 150090, China*
[2]*Department of Structural Engineering, University of California–San Diego, La Jolla, California 92093-0085, USA*

(Received 1 May 2013; accepted 3 July 2013; published online 22 July 2013)

Behaviors of liquids in two-dimensional (2D), lyophobic nanoenvironment were investigated experimentally by using a surface-modified, graphene-based nanoslit composite (GBNC). Different from previous reports on one-dimensional (1D) nanofludic behaviors, the infiltration pressure of 2D nanofluid is not dependent on the infiltration volume, leading to a flat infiltration plateau in the sorption isotherm curve. This unique phenomenon implies that, compared with a 1D nanoenvironment, more energetically favorable molecular configurations may be formed in a 2D nanoslit, probably due to the relaxation of the lateral confinement. © *2013 AIP Publishing LLC*. [http://dx.doi.org/10.1063/1.4816095]

I. INTRODUCTION

Fluid transportation in nanoenvironment has been an important topic of research in a variety of scientific and engineering fields, such as biotechnology and advanced sensing and actuation.[1,2] It was discovered that a fluid confined in a nanostructure exhibits unique characteristics, such as the "grainy" structure,[3] the "single-file" transport phenomena,[4] and the enhanced flow rate.[5–7] A large number of nanofluidic devices, including nanochannels, nanoarrays, nanolameli, and nanoslits,[8–12] have been developed and employed for material separation, thermal and electrical conduction, biosensor, fluid transportation, and fuel cell fabrication,[13–18] among others.

Recently, the application of nanofludic systems were extended to the area of advanced structures, particularly energy absorption materials and structures (EAMS).[19–21] In such systems, when liquid molecules were forced to enter and "flow" inside lyophobic nanochannels, the effective nanocapillary force must be overcome, and, thus, the input energy was either dissipated or "captured."[22,23] A modified Laplace-Young equation was developed to calculate the required infiltration pressure.[24] In many of these EAMS nanofluidic systems, once the liquid entered the nanochannels, the confined phase would be "locked" inside.[25] The irreversible nanoflow provided a promising mechanism for the development of high-performance protection devices, while not relevant to damping equipments, which must repeatedly work under cyclic loadings. A few nanoporous silica-based nanofludic systems were developed,[26,27] in which the confined liquid can defiltrate spontaneously as the external loading are lowered. Their performance in engineering practice is still being under investigated. In addition, a carbon nanotube (CNT)-based nanofludic system was developed,[28] where water molecules could enter into the nanotubes from both ends, suggesting that such an arrangement may be suitable to applications associated with continuous liquid flows.

Most of the above mentioned research, including both experimental and theoretical analyses, is focused on one-dimensional (1D) phenomena, e.g., confined liquid performance in nanotubes, nanopores, or nanochannels. In a 1D confining nanoenvironment, the liquid molecules are constrained from all the directions, and, therefore, the system free energy may be higher than otherwise. The liquid infiltration pressure is dependent on effective interfacial tension, molecular potentials, nanopore/nanotube diameter, effective "flow" rate,[23] as well as external thermal and electric fields.[24–29] The system free energy is also a function of the effective infiltration depth, due to the unique "column resistance."[24]

It is envisioned that, if some degrees of freedom of lateral motion are given to the confined liquid molecules, more energetically favorable configurations may be achieved as the molecules move inside a two-dimensional (2D) confining nanoenvironment, such as a nanoslit. In this paper, we conduct an experimental investigation on a graphene-based system. Useful testing data are measured and discussed.

II. EXPERIMENTAL

A. Graphene preparation

A graphite material synthesized through a modified surface conditioning method[30] was employed as the precursor of graphene-based nanoslit composite (GBNC). About 3 g of purified 325 mesh graphite (XFNANO, NO. XF010) was mixed with 2.5 g of sodium nitrate and 120 ml of 95 wt. % H_2SO_4 by magnetically stirring for 30 min in an ice bath, with 15 g of potassium permanganate being slowly added. After 12 h, the bright-yellow suspension was diluted with 150 ml H_2O and refluxed in an oil bath for 24 h. Finally, the mixture was treated by H_2O_2 (50 ml, 30 wt. %) and then

[a)]Author to whom correspondence should be addressed. Electronic mail: lihui@hit.edu.cn.

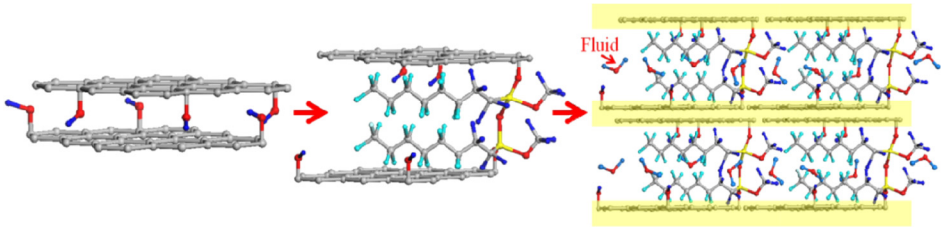

FIG. 1. Processing of GBNC: (a) untreated GOs, (b) functionalized GOs, and (c) GBNC.

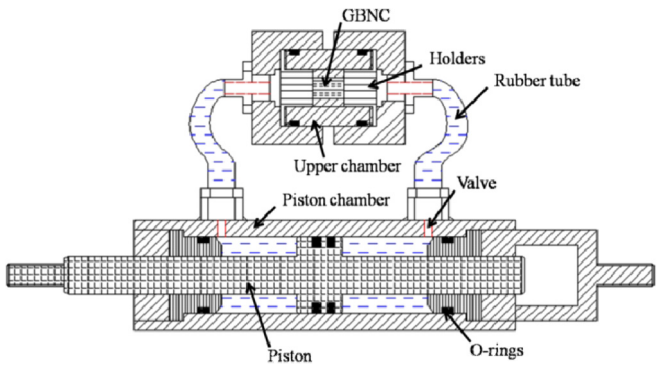

FIG. 2. Diagram of the experimental setup for the pseudostatic and dynamic testing.

diluted with distilled water and 5 wt. % HCL, respectively, to remove the manganese ion. Due to the small interlayer distance (d-spacing) of graphene, only water molecules could pass through the graphene oxide (GO) membranes.[31]

In order to enlarge the d-spacing and achieve a high two-dimensional nanocapillary force, long-chain-length silane groups (Dodecafluoroheptylpropyltrimethoxysilane)[28] were grafted onto the monolayer GOs. First, the fabricated GOs were dissolved in 2 l distilled water and centrifuged (4500 rpm, 15 min) until the pH value was neutral. After being vacuum dried at 90 °C, about 1 g GOs were dispersed in 100 ml of dry toluene by ultrasonic method. Then, 20 ml of the long-chain-length silane was added together with 1 ml

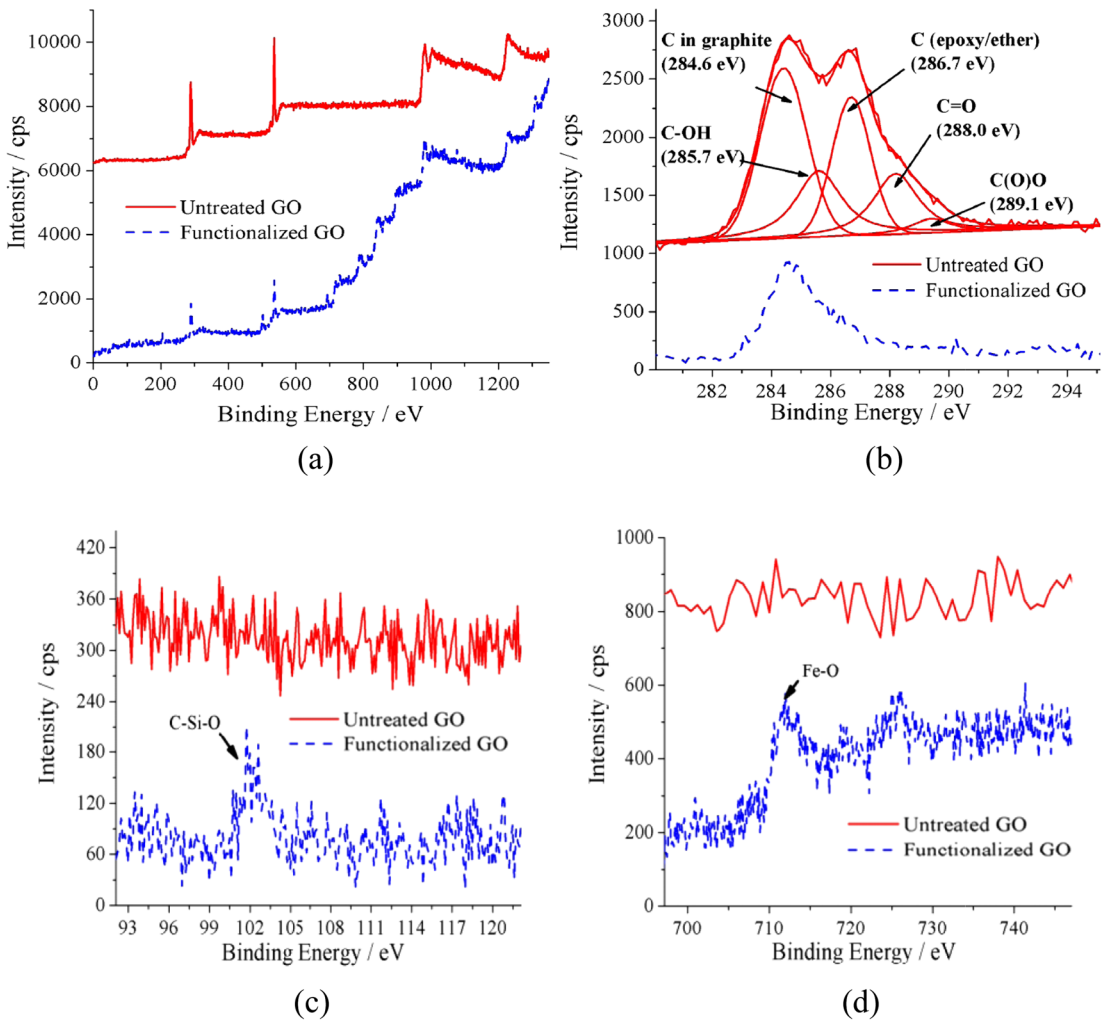

FIG. 3. XPS results of GOs: (a) total spectra, (b) C spectra, (c) Si spectra, and (d) Fe spectra.

of 5 wt. % HCl. The mixture was refluxed at 90 °C in an oil bath for 24 h and vacuum dried at 60 °C for 12 h.

To form an aligned nanoslit composite, GOs were magnetized by decorating Fe_3O_4 nanoparticles on their surfaces. Hydrophobic GO and ferrous sulfate particles were sealed in a flask with a mass ratio of 1:10. Then, a solvent, composed by distilled water and ethanol with the volume ratio of 4:1, was injected into the flask and the mixture was ultrasonically dispersed for 15 min and mechanically stirred for 6 h, followed by the addition of NaOH particles, with the molar concentration two times higher than that of the ferrous sulfate. Finally, the mixture was stirred and refluxed at 90 °C in an oil bath for 6 h and vacuum dried.

B. Composite processing

Different from the regular GOs, the functionalized materials were in powder form and could not form membranes by self-condensation. Thus, bisphenol-A epoxy resin was employed to bind the multilayer GO particles, so as to form a GBNC. GOs, bisphenol-A epoxy resin and its room-temperature curing agent, with a mass ratio of 1:1:0.25, were dissolved in 50 ml acetone. Being stirred at room temperature, acetone volatilized continually. Then, the mixture was placed into a 5 mm depth cylindrical mold under a 1 T oriented magnetic field, at 80 °C for 6 h. Finally, surfaces of the composite, perpendicular to the magnetic field, were polished by a lathe with acetone as the wetting agent, to open the entrances of the nanoslits. The entrances opening condition was characterized by Scanning Electron Microscope (SEM) on a Quanta 200 F system. Figure 1 depicts the schematic of the processing procedure.

C. Measurement of nanocapillary forces in 2D nanoslits

The GBNC sample was immersed in glycol, forming a nanofluidic system. Figure 2 depicts the experimental setup. A stainless steel upper chamber, 70 mm in length and 32 mm in inner diameter, and a stainless steel lower piston-chamber, 200 mm in length and 45 mm in inner diameter, were placed together, with a GBNC sample sandwiched in between. A stainless steel piston was installed in the lower chamber. The diameters of the piston rod and the piston head-block were 32 mm and 45 mm, respectively. The GBNC sample was mounted at the center of the upper chamber by two steel sieve holders. The cell size of the sieve holder was about 0.1 mm. The chambers were connected to each other by high pressure rubber tubes, sealed by polytetrafluoroethylene o-rings, as depicted in Figure 2. Before loading test, the setup was filled with glycol and the trapped air was pumped out via venting valves.

By moving the stainless steel piston back and forth in the lower chamber, the liquid phase was forced to flow across the GBNC sample repeatedly. Quasi-static (0.005 Hz) and dynamic (0.1 and 0.5 Hz) loading tests were carried out. The load was applied and measured by a Type 4505 Instron machine in a step-wave displacement control mode for the quasi-static tests, and a sine-wave displacement control mode for the dynamic tests. The maximum displacement of the step wave and the sine wave was 5 mm.

D. Materials charactering

The functionalized GOs were characterized by X-ray photoelectron spectroscopy (XPS), X-Ray Diffractomer (XRD), and Transmission Electron Microscope (TEM) by a PHI 5700 ESCA System, a D/max-rb, and a Tecnai G2 F30 device, respectively.

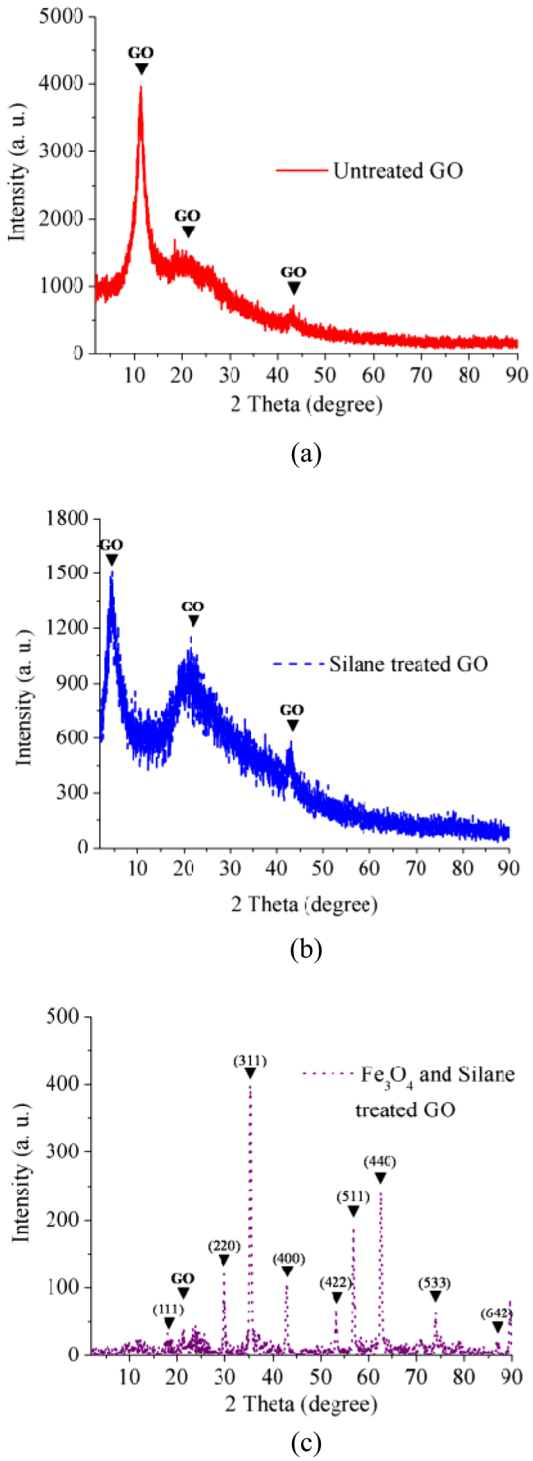

FIG. 4. XRD results of GO: (a) untreated GOs, (b) silane treated GO, and (c) Fe_3O_4 and silane treated GO.

III. RESULTS AND DISCUSSION

A. Results of materials characterization

In the functionalized GO, there is one silicon atom in each hydrophobic chain and three ferrum atoms in each Fe_3O_4 molecule. Thus, silicon and ferrum contents are used to evaluate the treatment effectiveness of silane groups and Fe_3O_4, respectively. From the XPS data, as shown in Figure 3(a), the untreated GOs have only negligible silicon and ferrum contents, while there are evident silicon and ferrum peaks in the spectrum for the treated graphenes. In the C spectra (Figure 3(b)), regular peaks of oxygen groups on untreated GOs can be clearly observed.[32] Once treated by silane groups and Fe_3O_4 nanoparticles, a considerable portion of hydroxyl and epoxy sites is deactivated. Figures 3(c) and 3(d) show that the Si and Fe spectra and the peaks of C-Si-O and Fe-O bonds can be, respectively, observed at the binding energies of 102.4 and 712.5 eV, indicating that they have been chemically bonded. According to the XPS data, the atomic concentrations of silane groups and Fe_3O_4 are about 5.53% and 2.05%, respectively.

The structures of the untreated and functionalized GOs were also characterized via XRD analysis. A regular GO would have a 2θ peak at 11.32 degrees,[33] which indicates a d-spacing about 0.78 nm,[34,35] as shown in Figure 4(a). As the GO is treated by silane chains, a low intensity 2θ peak can be observed at about 4.36 degrees, corresponding to a mean d-spacing around 1.96 nm; that is, the d-spacing is significantly increased.[36–38] Figure 4(c) shows the data of the Fe_3O_4 and silane treated GOs, presenting the diffraction peaks of the face-centered cubic crystals of Fe_3O_4 (JCPDS 19–0629). However, no Si or F peaks can be detected, implying that the grafted silane chains formed amorphous structures.

TEM results are shown in Figures 5(a)–5(d). The untreated GOs are in regular monolayer form (Figure 5(a)), while the monolayers of the treated GOs tend to link each other, resulting in a multilayer structure (Fig. 5(b)), possibly aided by the self-polycondensation of silane chains. The elemental mapping of Si shown in Figure 5(b) indicates that the distribution of the grafted silane chains on the GOs is quite uniform. According to Figures 5(c) and 5(d), the decorated ferroferric oxide phase is homogeneous, with a cluster size ranging from about 5 to 50 nm, assessed from Figure 5(c).

Figure 6 shows the SEM images of a GBNC. Because of self-condensation, untreated GOs spontaneously form membranes with the d-spacing of 0.78 nm (Figure 6(a)). To form a GBNC with an increased d-spacing, the hydrophobic GO powders are magnetized with Fe_3O_4 nanoparticles and mixed with epoxy resin. Under an oriented magnetic field, most of the functionalized GOs are aligned quite well (Figure 6(b))

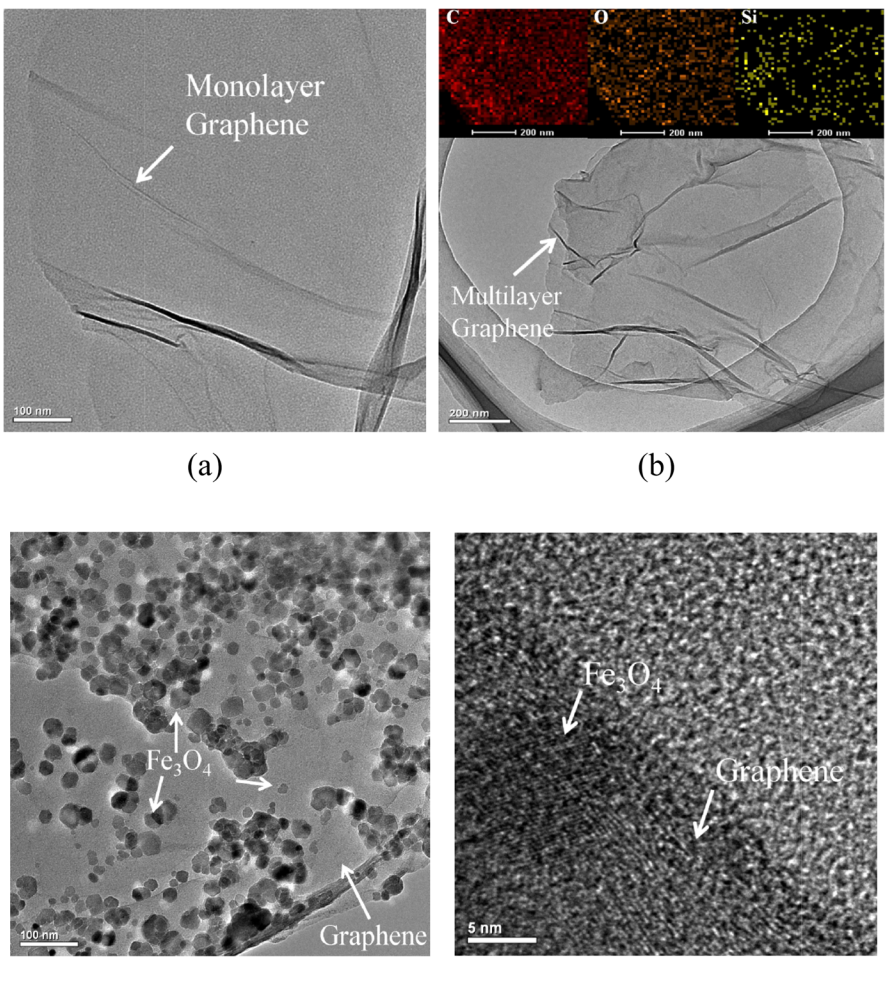

FIG. 5. TEM images of GOs: (a) TEM image of untreated monolayer GOs, (b) TEM image of silane treated GOs, (c) TEM image of Fe_3O_4 and silane treated GOs, and (d) high resolution TEM image of the final functionalized GOs.

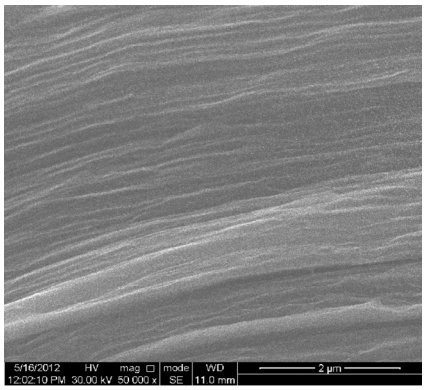

(a)

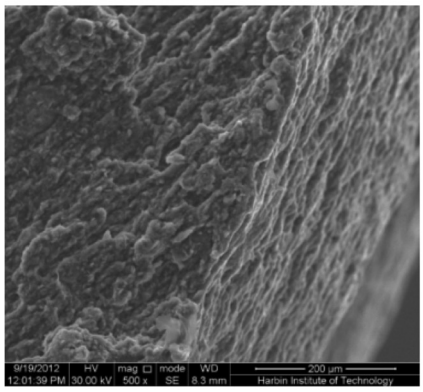

(b)

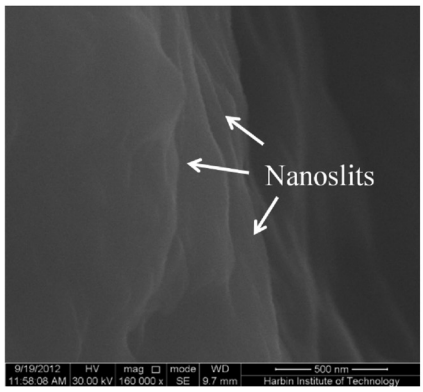

(c)

FIG. 6. SEM images of graphene-based composite: (a) SEM image of untreated GOs formed membranes, (b) SEM image of the functionalized graphene-based composite, and (c) SEM image of the formed regular nanoslit structures.

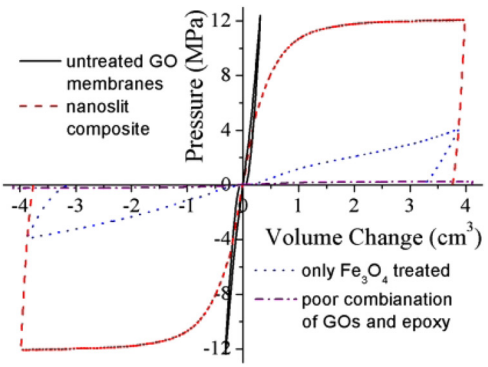

(a)

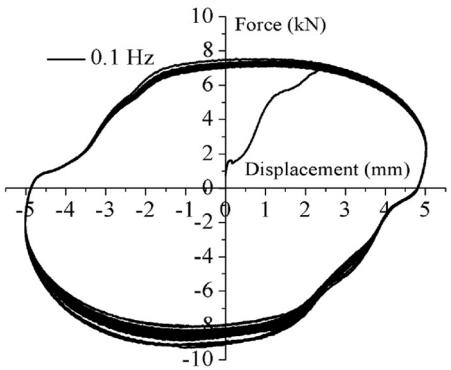

(b)

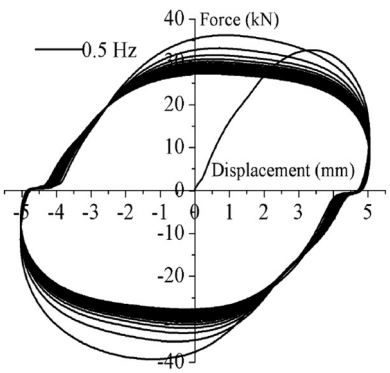

(c)

FIG. 7. Damping behavior of the nanofluidic material: (a) pseudostatic testing sorption isotherm curves, (b) dynamic hysteretic curves at 0.1 Hz, and (c) dynamic hysteretic curves at 0.5 Hz.

and the entrances of nanoslits are exposed at sample edges, shown in Figure 6(c).

B. Measurement of nanocapillary force in 2D nanoslit

In the quasi-static tests, the piston was moved at a low frequency of only 0.005 Hz. From the sorption isotherm (the red dash line in Figure 7(a)), it can be seen that the curve is quite linear when the load is small, which can be attributed to the compression of liquid phase as well as the machine compliance. As the pressure increases and reaches about 11 MPa, the liquid begins to enter and pass through the nanoslits in the GBNC sample continuously. As a result, an infiltration plateau is formed. A similar pressure plateau is formed when the liquid is forced to go back, as the piston is moved backward. In 1D nanotubes and nanopores, the infiltration plateaus were never flat: as more and more liquid molecules enter the nanoenvironment, the resistance of the tube/pore walls becomes increasingly pronounced, and, thus, the effective capillary force rises considerably.[24,26] In this experiment on the 2D nanoslits, the slope of the infiltration plateau is nearly zero, implying that the relaxation of the constrains from the lateral directions on the confined liquid

molecules significantly reduces the system free energy, promoting the formation of more energetically favorable molecular configurations, which is consistent with the fast transport phenomenon in the graphene nanoribbon-guided fluid channels.[39]

For the surface untreated GO membranes, as suggested by the black solid curve in Figure 7(b), if the d-spacing of GOs is not enlarged, glycol cannot pass through the membranes even at a much higher pressure. The behavior of GOs modified by only Fe_3O_4, as shown in Figure 7(b) (the blue dotted line), indicates that glycol can relatively easily pass through the magnetized graphene-based composite. The purple dashed dotted line in Figure 7(b) denotes the behavior of the liquid in another set of reference samples, in which the nanoslit composite and epoxy are not tightly bonded. The liquid can pass through the gaps between nanoslits and epoxy quite easily, such that the infiltration pressure is much lower. Hence, the high capillary forces measured on the GBNC sample around 11 MPa must be attributed to the liquid motions inside the lyophobic grapheme-based nanoslits.

In the dynamic tests, to adjust the infiltration pressure, the liquid was 40% ethanol solution of glycol. The loading frequency was in the range from 0.1 to 0.5 Hz. From the testing data shown in Figures 7(b) and 7(c), it can be seen that the maximum driving force of the nanofluidic structure increased from about 7 to 30 kN; that is, the infiltration pressure increased from about 8.75 to 37.33 MPa, as the loading frequency was raised from 0.1 to 0.5 Hz. After a few loops, the hysteretic converged to a steady-state, suggesting that the capillary forces associated with the cyclic "flow" in the 2D nanoslits can be achieved repeatedly. According to the parallelogram-like hysteretic curves, even under the cyclic "flow" conditions, the infiltration plateau are quite flat, obviously distinct from the characteristics of 1D nanofluidic behaviors.

Compared with many conventional viscous and viscoelastic materials,[40,41] the infiltration pressure, i.e., the "yielding stress," of the GBNC system is much higher. Therefore, with the same volume and weight, a much larger energy dissipation efficiency can be achieved, which may provide a potential way for developing high-performance damping components for civil and mechanical structures.

IV. CONCLUSIONS

In summary, liquid "flow" in a 2D nanoenvironment was investigated through a set of experiments on GBNC. Different from the reported pressure increase in 1D nanotubes or nanopores, the infiltration pressure of the 2D nanofluidics does not increase as the infiltration volume rises, suggesting that the "column resistance" associated with 2D nanofluidic behavior is negligible. This may be attributed to the relaxation of the lateral confinement, so that more energetically favorable molecules configurations can be formed. The infiltration pressure can be quite high, compared with that of conventional damping materials and systems, and quite stable as the loading-unloading cycles are repeated.

ACKNOWLEDGMENTS

This work was supported by the Ministry of Science and Technology of China under Grant No. 2011BAK02B02.

[1]S. Prakash, M. Pinti, and B. Bhushan, Philos. Trans. R. Soc. London, Ser. A. **370**, 2269–2303 (2012).
[2]A. Piruska, M. Gong, J. V. Sweedler, and P. W. Bohn, Chem. Soc. Rev. **39**, 1060–1072 (2010).
[3]J. C. Rasaiah, S. Garde, and G. Hummer, Annu. Rev. Phys. Chem. **59**, 713–740 (2008).
[4]G. Hummer, J. C. Rasaiah, and J. P. Noworyta, Nature (London) **414**, 188 (2001).
[5]M. Majumder, N. Chopra, R. Andrews, and B. J. Hinds, Nature **438**, 44 (2005).
[6]S. Joseph and N. R. Aluru, Nano Lett. **8**(2), 452–458 (2008).
[7]J. K. Holt *et al*., Science **312**, 1034-1037 (2006).
[8]P. Abgrall and N. T. Nguyen, Anal. Chem. **80**, 2326-2341 (2008).
[9]Z. Ma, T. Kyotani, Z. Liu, O. Terasaki, and A. Tomita, Chem. Mater. **13**(12), 4413–4415 (2001).
[10]M. D. Gregory, Prog. Mater. Sci. **55**(7), 629–674 (2010).
[11]F. López-Tejeira, S. G. Rodrigo, L. Martín-Moreno, F. J. García-Vidal, E. Devaux, T. W. Ebbesen, J. R. Krenn, I. P. Radko, S. I. Bozhevolnyi, M. U. González, J. C. Weeber, and A. Dereux, Nat. Phys. **3**, 324–328 (2007).
[12]D. Mijatovic, J. C. Eijkel, and A. van den Berg, Lab Chip **5**(5), 492–500 (2005).
[13]M. A. Shannon, P. W. Bohn, M. Elimelech, J. G. Georgiadis, B. J. Marinas, and A. M. Mayes, Nature **452**, 301-310 (2008).
[14]M. Napoli, J. C. Eijkel, and S. Pennathur, Lab Chip **10**(8), 957–985 (2010).
[15]S. J. Kim, Y. A. Song, and J. Han, Chem. Soc. Rev. **39**(3), 912-922 (2010).
[16]P. Dutta and J. Morse, Recent Pat. Nanotechnol. **2**(3), 150–159 (2008).
[17]E. S. Choi, J. S. Brooks, D. L. Eaton, M. S. Al-Haik, M. Y. Hussaini, H. Garmestani, D. Li, and K. Dahmen, J. Appl. Phys. **94**(9), 6034–6039 (2003).
[18]C. Y. Lee, W. Choi, J. H. Han, and M. S. Strano, Science **329**, 1320–1324 (2010).
[19]F. B. Surani, X. Kong, and Y. Qiao, Appl. Phys. Lett. **87**, 251906 (2005).
[20]X. Xu, H. Li, and G. Xian, Mater. Lett. **66**, 176–178 (2012).
[21]L. Liu, H. Lim, W. Lu, Y. Qiao, and X. Chen, Appl. Phys. Express **6**, 015202 (2013).
[22]A. Han and Y. Qiao, J. Phys. D: Appl. Phys. **40**, 3436–3439 (2007).
[23]X. Chen, G. Cao, A. Han, V. K. Punyamurtula, L. Liu, P. J. Culligan, T. Kim, and Y. Qiao, Nano Lett. **8**, 2988–2992 (2008).
[24]Y. Qiao, L. Liu, and X. Chen, Nano Lett. **9**, 984–988 (2009).
[25]A. Han, W. Lu, T. Kim, X. Chen, and Y. Qiao, Phys. Rev. E **78**, 031408 (2008).
[26]A. Han and Q. Yu, Chem. Phys. Lett. **454**, 294–298 (2008).
[27]W. Lu, T. Kim, V. K. Punyamurtula, A. Han, and Y. Qiao, J. Mater. Sci. **46**, 4053–4057 (2011).
[28]H. Li, X. Xu, and T. Shi, Mater. Chem. Phys. **136**, 858–862 (2012).
[29]B. Xu, B. Wang, T. Park, Y. Qiao, Q. Zhou, and X. Chen, J. Chem. Phys. **136**, 184701 (2012).
[30]S. Gilje, S. Han, M. Wang, K. L. Wang, and R. B. Kaner, Nano Lett. **7**, 3394 (2007).
[31]J. S. Bunch, S. S. Verbridge, J. S. Alden, A. M. van der Zande, J. M. Parpia, H. G. Craighead, and P. L. McEuen, Nano Lett. **8**, 2458 (2008).
[32]S. Park, J. An, R. D. Piner, I. Jung, D. Yang, A. Velamakanni, S. T. Nguyen, and R. S. Ruoff, Chem. Mater. **20**(21), 6592–6594 (2008).
[33]D. A. Dikin, S. Stankovich, E. J. Zimney, R. Piner, G. H. B. Dommett, G. Evmenenko, S. T. Nguyen, and R. S. Ruoff, Nature **448**, 457–460 (2007).
[34]A. Buchsteiner, A. Lerf, and J. Pieper, J. Phys. Chem. B **110**, 22328–22338 (2006).
[35]A. Lerf, A. Buchsteiner, J. Pieper, S. Schottl, I. Dekany, T. Szabo, and H. P. Boehm, J. Phys. Chem. Solids **67**, 1106–1110 (2006).
[36]S. Park, K. S. Lee, G. Bozoklu, W. Cai, S. T. Nguyen, and R. S. Ruoff, ACS Nano **2**, 572–578 (2008).
[37]M. Fang, K. Wang, H. Lu, Y. Yang, and S. Nutt, J. Mater. Chem. **20**, 1982–1992 (2010).
[38]K. Raidongia and J. Huang, J. Am. Chem. Soc. **134**, 16528–16531 (2012).
[39]L. Liu, L. Zhang, Z. Sun, and G. Xi, Nanoscale **4**(20), 6279-6283 (2012).
[40]D. Lee and D. P. Taylor, Struct. Des. Tall Build. **10**, 311–320 (2001).
[41]R. H. Zhang and T. T. Soong, J. Struct. Eng. **118**(5), 1375–1392 (1992).